Simple and complex multidimensional actomyosin crossbridges

C.D. Williams, M. Regnier, T.L. Daniel

2009–06–25

Abstract

Existing spatially explicit models of muscle contraction treat myosin as a single spring oriented parallel to the direction of contraction. A model of myosin that incorporates multiple springs, forming a four spring crossbridge (4sXB), closely replicates the motions used in myosin's power stroke to generate force. This 4sXB model is able to take most of its parameters from experimental measurements and permits monitoring of phenomena not possible with a single-spring crossbridge. The 4sXB generates radial force during its power stroke similar to what a physical crossbridge produces. Also as with physical crossbridges, the 4sXB's kinetics and force production vary with lattice spacing as angles of attachment, crossbridge geometry and diffusion distances change. We also propose a simpler two spring crossbridge (2sXB) that replicates much of the 4sXB's desirable properties. Unlike the 4sXB, the length and angle of the springs comprising the 2sXB can be determined analytically for any chosen head position without the use of iterative techniques. Both the 4sXB and the 2sXB maintain similar kinetics to previous work at resting lattice spacings, permitting more direct comparison of work done with either system to previous studies. Lattice spacing dependent axial and radial forces are measured and considered.

Keywords: myosin; spatially-explicit model; crossbridge kinetics

1 Introduction

Theoretical and computational models of cross-bridge force generation have largely focused on one-dimensional analyses. Thus, from the early work of Huxley (1) to more recent models (2–4) our focus has been more on the force distribution along the filament lattice. From a computational standpoint, somewhat

less attention has focused on radial forces. That said the geometry of the single spring crossbridge has remained largely unchanged while the kinetics underlying transitions between force generating states have been increased in complexity throughout subsequent work. (2, 4, 5) Meanwhile, Houdusse and Sweeney (6) and others have proposed that the region of the lever arm directly adjacent to the converter region is a flexible area that acts as a spring. This model of force generation by myosin suggests that inclusion of torsional spring might create a system that better reflects the underling mechanisms of the powerstroke.

Here we analyze the properties of and compare two torsional spring based crossbridge models that are targeted for use in spatially explicit models of the half sarcomere. The first is a four spring crossbridge (4sXB) that is directly inspired by the structure of the S1 and S2 regions of myosin II. Following this, we consider a two spring crossbridge (2sXB) that replicates many of the behaviors of the 4sXB while requiring fewer computational resources.

2 Materials and Methods

We consider two crossbridge models meant to capture a range of mechanical behaviors suggested by the literature. Each, described more fully below can be derived from a generalized crossbridge consisting of 4 springs: two torsional springs and two linear springs (Fig 1). These are contrasted to the traditional one-dimensional single spring model of a crossbridge.

Geometry

Spring configurations Our simplest model consists of a single linear spring aligned parallel to the thick and thin filaments, existing in one dimension. This one spring crossbridge (1sXB) is, as described above, the current crossbridge model implemented in most computational analyses. The one-dimensional 1sXB is insensitive to changes in lattice spacing, and unable to account for radial forces generated during axial shortening.

Our generalized four spring crossbridge (4sXB) uses two linear and two torsional springs to represent the myosin head, as depicted in Fig 1D. This allows the springs used in the model to closely correspond to pieces of the crossbridge. Specifically the four springs correspond to the S2/rod attachment point, the S2 region, the S2/light chain domain (LCD) attachment point, and the LCD. The use of multiple springs by the 4sXB also allow it to represent properties of the crossbridge that are only present in two dimensional space, in contrast to the one-dimensional 1sXB. The rest angle of the torsional spring linking the S2

domain and the LCD simulates the powerstroke by increasing during the transition from a weakly bound to a strongly bound state. This two dimensionality allows the 4sXB to be embedded in a space that takes the distance between thick and thin filaments into account, introducing lattice spacing dependence.

The 2sXB uses one linear and one torsional spring to represent the myosin head, (Fig. 1C). This crossbridge is a simplified version of the 4sXB, retaining movement generated by a lever arm, but altering the length of the lever such that it can bridge the entire distance between the thick and thin filaments. The parameters characterizing the 2sXB are chosen to match the step size and kinetics of the 2sXB to those of the 4sXB.

Parameters for both crossbridges are derived, where possible, from existing physical measurements. Each linear spring (one in the 1sXB, two in the 4sXB and one in the 2sXB) requires a rest length and spring constant, while each torsional spring (two in the 4sXB and one in the 2sXB) requires a rest angle and spring constant. The lengths and angles of the springs used for the 4sXB are chosen from tomographic reconstructions of in vivo S2 lengths and x-ray crystallographic reconstructions of the S1 fragment (7, 8). The rest length and angle of the 2sXB are set so that the tips of the 2sXB and 4sXB are in the same location before and after the powerstroke.

Calculation of lattice spacing Needs to be filled in with the following:

- Define rest lattice spacing
- Define range of typical lattice spacings
- Show offset calculation from known d_{10} of least radial force
- Should cite Millman in offset derivation also

Displacement and force generation Based on earlier mechanical models of force generation (e.g. Pate and Cooke; Daniel et al; Tanner et al.) each crossbridge undergoes a distortion upon the hydrolysis of ATP to ADP.Pi. That distortion changes the effective rest length of the crossbridge by an amount proportional to the energy derived from the hydrolysis. Within the 1sXB, this distortion is accomplished by a change in the rest length of the crossbridge's spring, while the 4sXB and 2sXB represent the distortion with a change in the rest angle of a torsional spring, a process more closely replicating the lever-arm mechanism (**?**). Upon release of Pi, distortional strain energy drives force generation by the crossbridge, essentially appearing as a change in the rest length of the molecule.

Calculation of spring lengths and angles When the 1sXB is placed under strain such that the myosin head is horizontally offset from the thick filament attachment site relative to its resting position, the length of the 1sXB's spring is simple to find as it must completely span the head to thick filament attachment distance. The lengths and angles of the springs in the 2sXB and 4sXB must take into account the radial distance they must cover as well. The 2sXB may be analytically determined, as it has all spring values set by the choice of a head location, with arm length and angle given by $r(h_x, h_y) = (h_x^2 + h_y^2)^{1/2}$ and $\theta(h_x, h_y) = \arctan(h_y/h_x)$, respectively. The 4sXB's greater number of degrees of freedom mean it requires iterative optimization to find the location of the distal torsional spring representing the link between the S2 and S1 regions when the crossbridge's head is moved to a new location. We use a modification of Powell's "dog-leg" method, present in the SciPy package of computational tools (9), to relax the location of the distal torsional spring to that which results in the lowest energy state of the 4sXB. Once the distal torsional spring's location is known (as (c_x, c_y)), the angle of the proximal torsional spring and the lengths of the two linear springs are determined analytically. The angle of the proximal torsional spring is given as $\phi(c_x, c_y) = \arctan(c_y/c_x)$, the length of the proximal linear spring as $\ell(c_x, c_y) = (c_x^2 + c_y^2)^{1/2}$, the angle of the distal torsional spring as $\theta(c_x, c_y, h_x, h_y) = \arctan((h_y - c_y)/(h_x - c_x)) + \pi - \phi(c_x, c_y)$, and the length of the distal linear spring as $r(c_x, c_y, h_x, h_y) = ((h_x - c_x)^2 + (h_y - c_y)^2)$.

Kinetics

We choose to use a simplified three state model of the crossbridge cycle (4, 5). This simplified system directly links the crossbridge's kinetics to mechanics; the three kinetic states are directly comparable to the myosin configurations described in Houdusse et al. (10). A secondary benefit of a three state kinetics system is that it allows multiple-motor models which use our many-spring crossbridges to more easily compare their results to those from the aforementioned previous models.

The three states represented in our kinetics are (1) an unbound state (2) a loosely-bound state and (3) a tightly-bound force-generating state. These states correspond to a Myosin-ADP-Pi state, an Actin-Myosin-ADP-Pi state, and an Actin-Myosin-ADP state (Fig. 1A).

The kinetics of both the two spring and the four spring models are strain dependent and are essentially transforms of the free energy landscapes experienced by the crossbridges in their different states. These free energies are a function of the distortion necessary to move the point representing the crossbridge's head to the point where we presume a binding site to be. Examples of these free energy landscapes are visible in figures 2A and 2B, with cuts through them at the rest lattice spacing visible in figure 3A.

The binding of both the two and four spring crossbridges is determined by Monte-Carlo simulation of their diffusion as a result of being perturbed by Boltzmann derived energy distributions. After a new head location is found, a binding probability is calculated that decreases exponentially with distance from the potential binding site. This probability is tested against a random number from a uniform distribution to determine if binding occurs. This method is similar to that used by Tanner et al. (4).

Free energy in each state The total energy, liberated by the hydrolysis of a P_i, available to a crossbridge depends on the concentrations of ATP, ADP and P_i and is given by $\Delta G = -\Delta G_{0,ATP} - \ln \frac{[ATP]}{[ADP][P_i]}$. In weakly and strongly bound states a portion of that energy is available to the crossbridge, allowing the crossbridge at most 28% (in the weakly bound state) or 68% (in the strongly bound state) of ΔG for mechanical work (see efficiency factors $\alpha = 0.28$ and $\eta = 0.68$ below; Tanner et al. (4), Pate and Cooke (5)). The total free energy of a crossbridge in each state also depends on the strain that the crossbridge experiences from distortion upon binding. Thus the total free energy is a linear combination of the strain-dependent and phosphate-dependent energy of the crossbridge in each state. The free energy of the 4sXB system in each state is:

$$\begin{aligned}
U_1(\phi,\ell,\theta,r) &= 0 \\
U_2(\phi,\ell,\theta,r) &= \alpha\Delta G + \frac{k_\phi(\phi-\phi_0)^2 + k_\ell(\ell-\ell_0)^2 + k_\theta(\theta-\theta_0)^2 + k_r(r-r_0)^2}{2} \\
U_3(\phi,\ell,\theta,r) &= \eta\Delta G + \frac{k_\phi(\phi-\phi_0)^2 + k_\ell(\ell-\ell_0)^2 + k_\theta(\theta-\theta_1)^2 + k_r(r-r_0)^2}{2}
\end{aligned}$$

The free energy of the 2sXB system in each state is:

$$\begin{aligned}
U_1(r,\theta) &= 0 \\
U_2(r,\theta) &= \alpha\Delta G + \frac{k_r(r-r_0)^2 + k_\theta(\theta-\theta_0)^2}{2} \\
U_3(r,\theta) &= \eta\Delta G + \frac{k_r(r-r_1)^2 + k_\theta(\theta-\theta_1)^2}{2}
\end{aligned}$$

Binding rate calculation Our binding algorithm is descended from Tanner et al. (4) but differs in two key ways: we treat binding as a two step process and our diffusion step works with any number of springs. Binding depends on diffusion of the crossbridge head and proximity to the nearest binding site. Analogously, the process we use to simulate binding has two components, first the diffusion of the myosin head to a new location and then possible attachment to the nearest binding site (depending on the distance from the head and the binding site). The first step, diffusion, is simulated by thermally forcing each of a crossbridge's constituent springs with an energy plucked from a Boltzman distribution. This translates to assigning each spring a length or angle chosen

from the probability density function $P(x) = \sqrt{k/(2\pi kT)}\exp^{-(kx^2)/(2kT)}$ where x is the offset, k is the spring constant of the spring under consideration, and T is the system's temperature in Kelvin. We find the updated location of the crossbridge head from these new spring lengths and angles. The probability the crossbridge will form an attachment depends on the exponential of d, the distance from the crossbridge head's new location to the nearest binding site. Specifically, the probability of attachment is given by $p_{12}(d) = \gamma \exp^d$, where γ is a scaling factor chosen to provide attachment rates consistent with previous estimates. Attachment occurs if p_{12} is greater than *rand*, a number between 0 and 1 chosen from a uniform distribution. This process is used to determine whether a crossbridge binds during a single timestep; binding rates are calculated as the fraction of an ensemble of crossbridges that bind given the same starting conditions. Thus, for an ensemble of size n:

$$r_{12} = \frac{\sum_0^n \left(1 \text{ if } \gamma \exp^{-d} > rand, \text{ else } 0\right)}{n}$$

This two step system, with diffusion followed by a chance of attachment, is used for both the 4sXB and 2sXB with only a change in the number of thermally forced springs.

Powerstroke and detachment rates The powerstroke and detachment rates are based on the earlier work of Pate and Cooke (5) and Tanner et al. (4), and generalized here for the 4sXB and 2sXB in two-dimensional space. Both the powerstroke rate, r_{23}, and the detachment rate, r_{31}, are distortion dependent as they contain a term based on the differences in free energy between the current state and the one being considered for transition. This means that transitions are more likely when they are energetically favorable and less likely in other circumstances, a natural scheme based in the geometry of the crossbridges. The particular rates are as follows for both the 4sXB and the 2sXB:

$$r_{23}(U_2, U_3) = 0.001 + 0.5 * (1 + \tanh(0.6(U_2 - U_3)))$$

$$r_{31}(U_3, U_1) = e^{-1/(U_3 - U_1)}$$

Calculation of reverse rates Reverse transition rates are given by the thermodynamically balancing formula $r_{ij}/r_{ji} = \exp^{U_i - U_j}$ where r_{ji} is the forward rate and r_{ij} is the reverse rate (see Daniel et al. (2), Tanner et al. (4), Pate and Cooke (5)). For the transition from a weakly bound state to an unbound state this requires that the reverse transition is again treated as a fraction of an ensemble of transition opportunities.

3 Results

The models we present here were developed to examine consequences of lattice spacing on crossbridge kinetics and two dimensional force production. Multi-spring crossbridges introduce lattice spacing dependence into force production and kinetics, and account for forces not aligned with the direction of contraction. As lattice spacing changes, the kinetics and forces of the 4sXB and 2sXB shift in either or both magnitude and axial offset.

Axial offsets, magnitudes, axial components and radial components The axial component of vector values, such as force, is the vector portion that lies along the axis of the thick and thin filaments. The radial component of a vector value lies perpendicular to the thick and thin filaments, orthogonal to the axial component.

Baseline value changes occur where the lowest points, the highest points, or simply the offset of a value is shifted with regard to that seen at rest lattice spacing. Baseline value changes manifest in, e.g., the lowered probability of any binding occurring at extreme lattice spacings. Key value offsets occur when maxima, minima, inflection points, or other landmarks of a value's profile are shifted axially from where they occur at rest lattice spacings. Key value offsets are reflected in phenomena such as the axial offset at which a powerstroke will occur becoming right shifted at higher lattice spacings for the 2sXB. In addition to these lattice spacing dependencies, we examine the ability of the 4sXB and the 2sXB to model the radial component of the force produced during the powerstroke.

At 34 nm d_{10}, the multi- and single-spring crossbridges have similar kinetics and energies The free energy, binding rates, powerstroke rates and detachment rates of the 4sXB and 2sXB at a lattice spacing of 34 nm d_{10} are similar to those of the 1sXB (Figure 3). This is because the kinetics and energies of the multi-spring crossbridges are derived from those of the single-spring crossbridge. The single-spring crossbridge kinetics and energies were modified to be independent of the number of springs in a crossbridge, instead depending on the free energy of the crossbridge head in its current location. The crossbridge properties of the 1sXB, 2sXB and 4sXB are shown together in figure 3, where the 1sXB values used are calculated as in figure 10 of Tanner et al. (4). Although the properties of the multi- and single-spring crossbridges are largely similar, some divergences do occur. The multi-spring crossbridges' binding rate is a wider distribution than the single-spring crossbridge's binding rate due to the multi-spring crossbridges' use of diffusion-based binding probabilities. This causes the 2sXB and 4sXB, when averaged over all offsets, to be less likely

to bind but also to be more likely to bind at offsets with larger strains. The detachment rate of the single-spring crossbridge is its least energy-based value and required the most modification to function for all spring-based crossbridges. The detachment rate thus differs more than other rates or energies between the single- and multi-spring crossbridges. Despite these differences, many of the properties of the single-spring crossbridge are retained through the modifications which generalize the kinetics to two and higher dimensions.

Axial offset of most crossbridge properties decrease as lattice spacing increases The axial offset of most energies and kinetics of the 4sXB and 2sXB decreases as lattice spacing grows larger. The axial offset of a crossbridge property is the distance from the thick filament attachment site to that property's extremum or point of inflection at a given lattice spacing. An example of this change in axial offset is visible in subfigures 2a and 2b where the lowest energy point that the 4sXB or the 2sXB may reach at a lattice spacing of 32 nm d_{10} is more than 3 nm further from the crossbridge's thick filament attachment point than the lowest energy point reachable at a lattice spacing of 38 nm d_{10}. This offset-lattice spacing rule alters the behavior of the crossbridge with changes in lattice-spacing. The decreased chance of large axial offset binding occurring at larger lattice spacings decreases the chance of forward biased binding of the crossbridges at large lattice spacings (figures 2c and 2d). Similarly, the decreased axial offset of likely powerstrokes at larger lattice spacings causes the multi-spring crossbridges to have a smaller powerstroke at expanded lattice spacings (figures 2e and 2f). The only crossbridge property where the axial offset doesn't decrease as lattice spacing increases is the detachment rate of the 4sXB, due to the post-powerstroke angle of the crossbridge's head (figure 2g). Combined, these effects can reduce the amount of force a crossbridge will generate at larger lattice spacings.

Probability of a crossbridge being in a bound state decreases as lattice spacing diverges from rest As lattice spacing moves away from its 34 nm d_{10} rest value, a crossbridge becomes less likely bind if unbound and more likely to detach if bound. As defined above, the rest lattice spacing is defined as the radial offset at which multi-spring crossbridges under no strain will come to rest. The rates of binding and detachment are dependent on the difference in free energy between the unbound state and the loosely bound state in the first case and between the tightly bound state and the unbound state in the second. Thus, as lattice spacing increases or decreases from that at which bound crossbridges are under the least strain, the energy differences between bound states and the zero-energy unbound state increase and the crossbridge becomes increasingly likely to transition to and remain in the unbound state (figures 2c, 2d, 2g and 2h). An example of this is that the lowest rate of detachment of the 4sXB is 39/sec at a lattice spacing of 34 nm d_{10} while at 38 nm d_{10} the

detachment rate only dips as low as 486/sec. This is likely, in models incorporating multiple crossbridges, to decrease the number of crossbridges generating force at larger lattice spacings. At smaller lattice spacings, crossbridge induced realignment of binding sites due to the greater possible step size of each crossbridge shown above may cancel this effect. As the powerstroke rates depend on the difference between two parabolic energy profiles fed into tanh, their maximum and minimum probabilities do not change with lattice spacing (figures 2e and 2f). The result of these changes in the multi-spring crossbridges' kinetics as lattice spacing diverges from its rest value, considered independently of realignment present in models which incorporate multiple crossbridges, is that individual crossbridges will spend less time in a bound state .

Forces at a given axial offset increase with lattice spacing As lattice spacing grows greater, the axial and radial forces at a given axial offset will become more positive as lattice spacing increases, trending from initial negative values, through offsets of little force, to very positive values (see Fig. 4). For the 4sXB a 10 nm axial offset at 35 nm d_{10} gives about half the axial and half the radial force as the same crossbridge produces at 38 nm d_{10}. A 2sXB at a 12 nm axial offset at 35 nm d_{10} gives about two thirds of the axial and radial forces it produces at 38 nm d_{10}. These energy landscapes also show that no lattice spacing is free of radial force, which is zero at the crossbridges' rest locations but does not remain so across all axial offsets at even the rest lattice spacing. While the forces of both the 4sXB and the 2sXB undergo similar trends of increasing forces with lattice spacings, the details of their force landscapes do differ as a result of their different spring geometries (see Figs. 4 and 4). How these differences will alter the results of multiple crossbridge models using either the 4sXB or 2sXB remains to be seen.

Radial forces are of the same order of magnitude as axial forces The radial and axial components of force, produced by a 4sXB or 2sXB that is moved from its rest position to an axial offset, are of the same order of magnitude (Fig. 4a–d). The angle of the force vectors presented in Figures 4a–d give an indication of the relative values of the axial and radial force components at each location. Points with overwhelmingly axial or radial forces produce nearly horizontal or vertical vectors. That few such vectors are present indicates that neither the axial nor the radial force is greatly dominating the force produced by the 4sXB or the 2sXB.

4 Discussion

Strain and force generation at the level of a single crossbridge depend on lattice spacing Lattice spacing greatly alters the kinetic landscape to which individual multi-spring crossbridges are subject. Complex, and not entirely easy to visualize interactions occur between different kinetic rates with varying lattice spacing. A single example of this is that, for the 2sXB, the small lattice spacing axial offsets that are most likely to bind are increasingly less likely to quickly complete a powerstroke, due to the shift in the powerstroke rate's inflection point. In addition to lattice spacing altering the interactions between kinetic rates, radial forces are found to be present at levels which often equal axial forces. Multiple spring crossbridges open new doors to explore the relationships between kinetics, lattice spacing, radial force and axial force.

Simplicity of the 2sXB may be desirable While the 2sXB does not exactly mirror the behaviors of the 4sXB, it does resemble them in most ways (as seen in figures 2, 3 and 4) and may be the best option for further use in spatially explicit models due to its low computational requirements. As mentioned in the methods section, whenever the head of the 4sXB is moved the position of the middle torsional spring, roughly equivalent to the convertor domain, must be found through an iterative technique. This imposes a computation cost that is small for a single crossbridge, but which make longer duration multifilament simulations untenable. These problems do not exist for the 2sXB which requires no such step. As the kinetics and force of the 2sXB system resemble those of the 4sXB system in most instances, with the exceptions of their differing lattice spacing dependencies of the powerstroke rate and precise force orientation at some of the more extreme offsets, it may prove to be a useful model system.

Increased fidelity to known structure and mechanisms The multiple spring crossbridges both have a far greater ability than single spring crossbridges to replicate the defining characteristics of muscle myosin structure and the lever arm mechanism of force generation. The 2sXB and the 4sXB both generate force through the changing of the rest angle of a torsional spring attached to a lever arm. This is closely analogous to the lever arm mechanism as it is understood and stands in contrast to the mechanism by which a single spring crossbridge replicates the powerstroke (6). The single spring crossbridge generates its force with an offset of the myosin head can also be thought of as the spring representing the crossbridge having a different rest length in the unbound state and the loosely bound state than it does in the tightly bound state. This offset or altered rest length is what determines the stroke distance of the single spring crossbridge and estimates of it have varied from as little as 1 nm to as large as 10 nm (needs citation). By treating the crossbridge as several components

instead of a single spring we are able to base input parameters on values that can be referenced to existing crystallography structures.

Step size varies with lattice spacing for a two spring crossbridge Inherent in the geometry of the 2sXB and the 4sXB is a change in step size with a change in lattice spacing. Step size at a given lattice spacing is defined as the axial distance a myosin head moves between pre- and post-powerstroke angles if unconstrained in the axial direction and allowed to settle into the position which minimizes the energy of the crossbridge. These changes in step size occur because the angle which a given axial movement subtends increases with decreasing lattice spacings. This scenario also depends on the linear spring between the myosin's pivot point and the thin filament changing in length to accommodate differing lattice spacings. The single linear spring of the 2sXB is the only means by which the 2sXB may span the distance from the single torsional spring to the thin filament and thus must change with lattice spacing. However, the 4sXB is also possessed of the torsional and linear springs which are more proximal to the thick filament. These additional springs also adjust with lattice spacing, allowing the location of the 4sXB's pivot point to alter so that the difference in step size with changes in lattice spacing is smaller, although still present. This is yet another factor that may alter the force generated at different lattice spacings, increasing the strain and probability of detachment shortly after completing the powerstroke at larger lattice spacings.

Modeled radial forces are too large to ignore Simulated radial forces for both the 2sXB and the 4sXB were of the same order as the axial forces being produced. Inclusion of these forces in future modeling efforts presents an opportunity to examine an type of interaction ignored by previous spatially explicit models. Experimental evidence for the existence of strong radial forces during contraction is provided, at the level of muscle fibers, by observations of lattice spacings during redevelopment of tension in Cecchi et al. (11). Spatially explicit explorations of how these forces are transmitted throughout the lattice, or what restoring force prevents the creation of an overly disordered lattice where radial forces kink thick and thin filaments out of their axial paths are possible with either presented crossbridge.

Figures

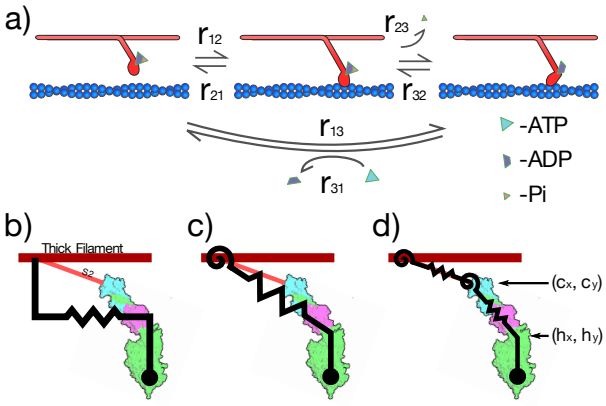

Figure 1: **Kinetic scheme and crossbridge types under investigation.** The three state kinetic system is shown in subfigure a. The three states represent (1) an unbound state, (2) a loosely bound state, and (3) a strongly bound state. The binding rate ($r_{1,2}$), strong transition rate ($r_{2,3}$), and unbinding rate ($r_{3,1}$) are determined by the energy stored in the springs representing the crossbridge. The reverse rates ($r_{2,1}$, $r_{3,2}$, and $r_{1,3}$) are functions of the forward transition rates. Subfigures b, c, and d show the representations of the crossbridge we examine, plotted against a myosin crystal structure for comparison. Subfigure b shows the single-spring crossbridge (1sXB) used heavily used in models since (1). Subfigure c depicts the two-spring crossbridge (2sXB) which uses both a torsional/angular spring and a linear spring. Subfigure d shows a four-spring crossbridge (4sXB) using two torsional and two linear springs, which we compare the single and dual spring crossbridges against. The locations of the distal torsional spring and tip of the 4sXB are denoted as (c_x, c_y) and (h_x, h_y) respectively. The tip of the 2sXB is also denoted as (c_x, c_y).

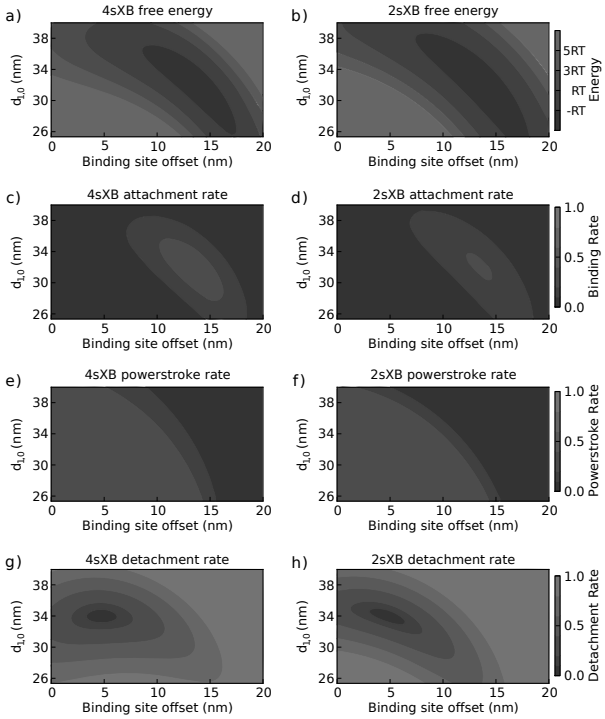

Figure 2: **Energy and kinetics of the 4sXB and 2sXB systems at varying axial offsets and lattice spacings.** Subfigures a through h show the properties of the 4sXB (subfigures a, c, e, and g) and the 2sXB (subfigures b, d, f, and h) as they change with binding site offset and $d_{1,0}$ lattice spacing. Binding site offset is the distance between the current axial location of the crossbridge's tip, h_x, and the location where the crossbridge attaches to the thick filament. Lattice spacing ($d_{1,-0}$) is defined as in Millman (12), with an offset to account for filament thicknesses so that the crossbridge exactly bridges the two filaments at a rest lattice spacing of 34 nm. Subfigure a depicts the free energy of the 4sXB at various lattice spacings (represented along the y-axis), with the head stretched to an axial offset from the thick filament attachment point (zero on the x-axis). Similarly, the free energy of the 2sXB is shown in subfigure b. The lowest energy myosin head locations in both a and b are shown as the darkest part of the plot and change in axial offset as lattice spacing changes. The subfigures c and d show $r_{1,2}$, the probability that the 4sXB and the 2sXB will transition from an unbound state to a bound state, and the dependence of this transition on both the axial offset of the open binding site from the myosin thick filament attachment site and the lattice spacing $d_{1,0}$ which is a function of the distance between the binding site and the thick filament attachment point of the myosin head. Subfigure c depicts this probability for the four spring crossbridge as a two dimensional contour with the same axes as a while subfigure d depicts the transition probabilities for the two spring crossbridge. Subfigures e and f show $r_{2,3}$, the probability of transition from a weakly bound state to a strongly bound state, for the same crossbridges, with the same axes and scales as c and d show $r_{1,2}$. Subfigures g and h show $r_{3,1}$, the probability of unbinding from a strongly bound state, for the same crossbridges, with the same axes and scales as c and d show $r_{1,2}$. The reverse rates, $r_{2,1}$, $r_{3,2}$, and $r_{1,3}$ may be back-calculated from the forward rates via the method described in (4).

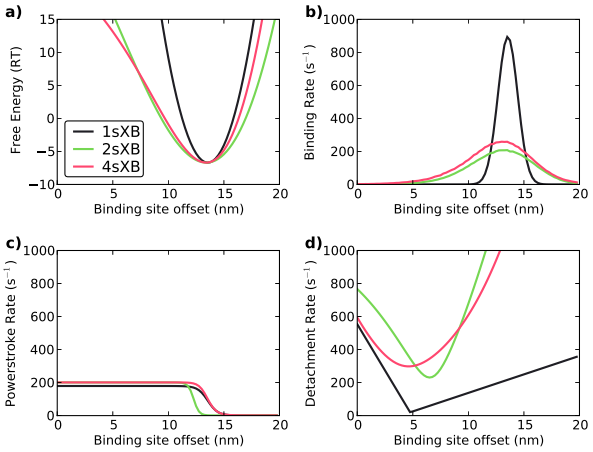

Figure 3: **Energy and kinetics of the 1sXB, 2sXB, and 4sXB at the resting lattice spacing.** Subfigures a through d show the energy and transition rates of the 1sXB (black line), 2sXB (green line), and 4sXB (red line) at resting lattice spacing. The 1sXB values shown for comparison are derived from those of Daniel et al. (2) and Tanner et al. (4), shifted axially so the resting location of the crossbridge head in each case is aligned with that of the 2sXB and 4sXB. The free energy of the crossbridges in state two is shown in subfigure a, where the multi-spring crossbridges' shifts from a strictly parabolic trajectory is visible. The explicit thermal forcing of the multi-spring crossbridge heads in subfigure b results in binding probabilities that are more distributed than those of the single spring crossbridge. The rate of powerstrokes, in subfigure c, remains least changed between the single and the multi-spring crossbridge models. The energy-based kinetics of the multi-spring crossbridges are least able to replicate the detachment rated of the 1sXB, as shown in subfigure d.

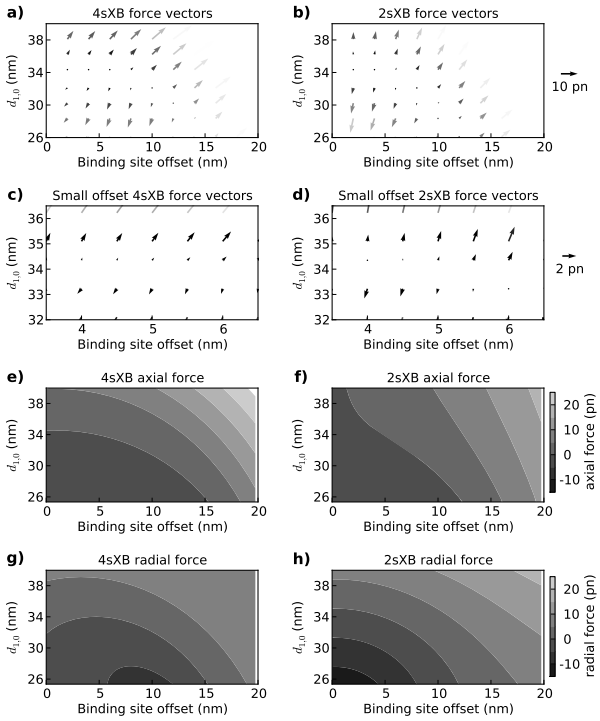

Figure 4: **Overview and detail of the forces exerted by the 2sXB and 4sXB.** Subfigures a through d show the forces exerted by the 4sXB and the 2sXB, with the shade of the vector arrows being determined by the chance of such a configuration occurring, a sum of the r_{23} and **the** the inverse of the r_{31} transition probabilities. Subfigures e through h show, separated, the axial and radial components of the 4sXB and the 2sXB. Subfigures a and b show overviews of the forces exerted, respectively, by the 4sXB and the 2sXB over lattice spacings and axial offsets that vary as in Figure 2. The forces exerted by the two crossbridges have radial components which frequently equal or exceed their axial components. A more detailed view of the region surrounding the rest position of the crossbridges is shown in subfigures c and d, where the large radial components of the crossbridge forces, particularly for the 2sXB, is again evident.

References

[1] Huxley, A., 1957. Muscle structure and theories of contraction. *Progress in biophysics and biophysical chemistry*

[2] Daniel, T., A. Trimble, and P. B. Chase, 1998. Compliant realignment of binding sites in muscle: transient behavior and mechanical tuning.

[3] Chase, P. B., J. M. Macpherson, and T. L. Daniel, 2004. A spatially explicit nanomechanical model of the half-sarcomere: myofilament compliance affects Ca(2+)-activation. *Annals of biomedical engineering*

[4] Tanner, B. C. W., T. L. Daniel, and M. Regnier, 2007. Sarcomere lattice geometry influences cooperative myosin binding in muscle. *PLoS Comput Biol*

[5] Pate, E., and R. Cooke, 1989. A model of crossbridge action: the effects of ATP, ADP and Pi. *J Muscle Res Cell Motil*

[6] Houdusse, A., and H. L. Sweeney, 2001. Myosin motors: missing structures and hidden springs. *Curr Opin Struct Biol*

[7] Taylor, K. A., H. Schmitz, M. C. Reedy, Y. E. Goldman, C. Franzini-Armstrong, H. Sasaki, R. T. Tregear, K. Poole, C. Lucaveche, R. J. Edwards, L. F. Chen, H. Winkler, and M. K. Reedy, 1999. Tomographic 3D reconstruction of quick-frozen, Ca2+-activated contracting insect flight muscle. *Cell*

[8] Rayment, I., W. Rypniewski, K. Schmidt-Bäse, R. Smith, D. Tomchick, M. Benning, D. Winkelmann, G. Wesenberg, and H. Holden, 1993. Three-Dimensional Structure of Myosin Subfragment-1: A Molecular Motor. *Science*

[9] Jones, E., T. Oliphant, P. Peterson, et al., 2001–.

[10] Houdusse, A., A. G. Szent-Gyorgyi, and C. Cohen, 2000. Three conformational states of scallop myosin S1. *Proc Natl Acad Sci USA*

[11] Cecchi, G., M. A. Bagni, P. J. Griffiths, C. C. Ashley, and Y. Maeda, 1990. Detection of radial crossbridge force by lattice spacing changes in intact single muscle fibers. *Science*

[12] Millman, B. M., 1998. The filament lattice of striated muscle. *Physiol Rev*